A study of in-situ sediment flocculation in the turbidity maxima of the Yangtze Estuary

Guo, Chao; He, Qing; Guo, Leicheng; Winterwerp, Johan C.

DOI
10.1016/j.ecss.2017.04.001

Publication date
2017

Document Version
Accepted author manuscript

Published in
Estuarine, Coastal and Shelf Science

Citation (APA)
Guo, C., He, Q., Guo, L., & Winterwerp, J. C. (2017). A study of in-situ sediment flocculation in the turbidity maxima of the Yangtze Estuary. *Estuarine, Coastal and Shelf Science*, *191*, 1-9.
https://doi.org/10.1016/j.ecss.2017.04.001

Postprint of Estuarine, Coastal and Shelf Science
Volume 191, 15 May 2017, Pages 1-9
Link to formal publication (Elsevier): https://doi.org/10.1016/j.ecss.2017.04.001

A study of in-situ sediment flocculation in the turbidity maxima of the Yangtze Estuary

Chao Guo[a], Qing He[a,*], Leicheng Guo[a], Johan C. Winterwerp[b]

[a] State Key Laboratory of Estuarine and Coastal Research, East China Normal University, Shanghai 200062, People's Republic of China

[b] Section of Environmental Fluid Mechanics, Faculty of Civil Engineering and Geosciences, Delft University of Technology, PO Box 5048, 2600 GA Delft, The Netherlands

Corresponding author: Qing He

Email address: qinghe@sklec.ecnu.edu.cn

Phone number: +86 (021) 6223 3688

Postal address: State Key Laboratory of Estuarine and Coastal Research, East China Normal University, Shanghai 200062, People's Republic of China

Highlights:

1. In-situ floc properties are examined in the turbidity maxima of the Yangtze Estuary.
2. Flocculation exhibits strong temporal and vertical variations over a tidal cycle.
3. Turbulence exerts major control on flocculation in this case.
4. Tidally varying flocculation has implication on siltation in the estuarine turbidity maxima.

Abstract

In order to improve our understandings of temporal and vertical variations of sediment flocculation dynamics within the turbidity maxima (TM) of the highly turbid Yangtze Estuary (YE), we deployed LISST-100C, a laser instrument for in-situ monitor of the sizes and concentrations of flocculated particles in a wet season. Field data in terms of vertical profiles of flow velocity, suspended sediment concentration (SSC), salinity, flocculated particle size distribution and volume concentration were obtained, based on field works conducted at consecutive spring, moderate, and neap tides.

Data analyses show that the mean floc diameters (D_M) were in the range of 14-95 μm, and flocculation exhibited strong temporal and vertical variations within a tidal cycle and between spring-neap cycles. Larger D_M were observed during high and low slack waters, and the averaged floc size at neap tide was found 57% larger than at spring tide. Effective density of flocs decreased with the increase of floc size, and fractal dimension of flocs in the YE was mainly between 1.5 and 2.1. We also estimated the settling velocity of flocs by 0.04-0.6 mm s^{-1} and the largest settling velocity occurred also at slack waters. Moreover, it is found that turbulence plays a dominant role in the flocculation process. Floc size decreases significantly when the shear rate parameter G is >2-3 s^{-1}, suggesting the turbulence breaking force. Combined effects of fine sediment flocculation, enhanced settling process, and high sediment concentration resulted in a large settling flux around high water, which can in part explain the severe siltation in the TM of the YE, thus shedding lights on the navigation channel management.

Keywords: Sediment flocculation; Floc settling; Turbidity maxima; the Yangtze Estuary.

1. Introduction

Flocculation plays an important role in cohesive sediment transport, which has been observed in various natural aquatic environments, including fresh and saline waters (Eisma, 1986; Droppo and Ongley, 1992; Dyer and Manning, 1999). Transportation of fine-grained suspended sediment is heavily dependent on the formation of flocs and their enhanced settling velocities which are orders of magnitude larger than that of the primary particles (Dyer, 1989; Whitehouse et al., 2000; Manning, 2004; Mehta, 2013). Therefore modelling and predicting cohesive sediment behavior demand good understandings of flocculation and floc settling processes (Soulsby et al., 2013). Since flocs are dynamic during transportation and they are highly fragile, traditional water sampling method may disrupt the flocs and unable to get the real properties of flocs in field. Hence in-situ instruments and techniques were needed and well developed, e.g., photography and video system (Eisma et al., 1990; Fennessy et al., 1994a; Manning and Dyer, 1999), and in-situ laser diffraction particle sizers (Agrawal and Pottsmith, 2000; Mikkelsen and Pejrup, 2001). The LISST (Laser In-Situ Scattering and Transmissiometry) is such an in-situ instrument widely used for flocculation studies (Mikkelsen and Pejrup, 2001; Fugate and Friedrichs, 2002; Xia et al., 2004; Curran et al., 2007; Guo and He, 2011; Markussen and Andersen, 2014). It is user-friendly and easy to handle in obtaining floc size distributions and volume concentrations. Moreover, LISST can be used to collect flocs information at different water depths and in a broader space scale, much easier and more quickly and cost efficient than using of cameras.

Brownian motion, differential settling, and fluid shears are three fundamental factors causing collision and aggregation of primary particles (Tsai et al., 1987). Many researches in the early periods had concluded that effects of Brownian motion on flocculation in estuarine and coastal environments were negligible (McCave, 1984; Partheniades, 1993; van Leussen, 1994). And the effect of differential settling was found much small through experiments by Stolzenbach and Elimelech (1994). Therefore, a number of researches focused on the effects of turbulent shears, turbidity, salinity, and biochemical processes on the development of flocs (Droppo and Ongley, 1992; Milligan and Hill, 1998; Winterwerp, 1998; Dyer and Manning, 1999; van Leussen, 1999). Fennessy et al. (1994b) reported that high current shears exert controlling influence on flocculation processes based on field data and Mietta et al. (2009) suggested that mean floc size increases with increasing organic matter content based on laboratory examinations and so on. van der Lee (2000) found that an increase in floc size with increasing suspended sediment concentration (SSC) in the Dollard Estuary, which disagrees with the results of Burban et al. (1989). Dyer (1989) provided a classical conceptual diagram on variations of floc size with SSC and turbulent shear, which showed that low shear promotes floc growth due to collision whereas a high shear leads to floc break-up, and the floc size increases with increasing SSC in quiescent water, however, larger flocs formed at higher concentrations are easily disrupted by shears. The conceptual model was confirmed by some works but did not meet all the situations and most of the researches were conducted in the low turbidity environments with SSC smaller than about 0.5 g l^{-1} (Milligan and Hill, 1998; Manning and Dyer, 1999; Xia et al., 2004; Markussen and Andersen, 2014; Sahin, 2014). It thus still needs more work in highly turbid systems to further extend our understandings of flocculation dynamics.

This study is devoted to examining flocculation in the estuarine turbidity maxima (TM) of the Yangtze Estuary (YE), a river- and tide-controlled muddy system with high SSC. Based on the laboratory and field researches, it was found that floc size increased with increase of SSC below 10 g l^{-1}, and the optimum salinity range for flocculation was 4-15‰ and the critical current velocity for flocculation was about 40-50 cm s^{-1} in the YE (Zhang et al., 1995; Guan et al., 1996; Jiang et al., 2002; Tang, 2007; Wan et al., 2015). But most of the existed researches in the YE were from lab experiments, and less research had been focused on the variation of flocculation through water column in spring-neap tidal cycles.

Training works in the North Passage (NP) of the YE in the aim to achieve a 12.5 m deep-water navigation channel lead to a huge amount of dredging requirement (60-100 million m^3 every year) (Xie et al., 2010; Song and Wang, 2013). It is thus eagerly to know where the sediments come from and how the sediments deposit in the

NP. Since the NP locates in the estuarine TM zone of the YE which is characterized by high SSC of fine sediment, understandings of flocculation processes and their impacts on sediment transport will benefit searching for answers of why siltation is such high in the NP. We aim to get a better understanding of flocculation dynamics in the estuary, and the purposes of this study are to reveal floc properties at different tidal phases in the TM of the YE, and identify its implications on the channel siltation from the point view of flocculation.

2. Field work and methodology

2.1. Introduction to the Yangtze Estuary

The YE is a meso-tidal estuary with a mean tidal range of 2.66 m and spring tidal range up to 5 m. The annual river flow is approximately 9,000 km^3 (1950-2010) at Datong, a station about 640 km landward the estuary mouth, and the water discharge at Datong is usually used to represent discharge to the YE. The mean and maximal water discharges in 2014 are about 28,000 $m^3\ s^{-1}$ and 56,300 $m^3\ s^{-1}$, respectively. And the decadal maximal discharge at Datong is 65,100 $m^3\ s^{-1}$ (2005-2014). The morphology of the YE is featured by three bifurcations and four outlets (see Figure 1a). The NP is now a man-made 12.5 m (below reference level) deep-water navigational channel. The NP is 92.2 km long and the observation site located in the middle part of this channel, where most back-silting occurred in recent years (Figure 1b).

The tide is irregularly semi-diurnal and the mean ebb tide duration is approximately 7.5 hours. Water depth is about 13 m (below mean water level) at the observation site and peak ebb and flood current velocities are 2.8 m s^{-1} and 1.8 m s^{-1} at spring tide, and peak ebb and flood velocities are 1.6 m s^{-1} and 1.2 m s^{-1}, respectively, at neap tide. The median diameters of suspended primary particles are mainly about 6-9 μm, and constitutes of particles include about 40% clay, 54% silt, and 6% sand in this area.

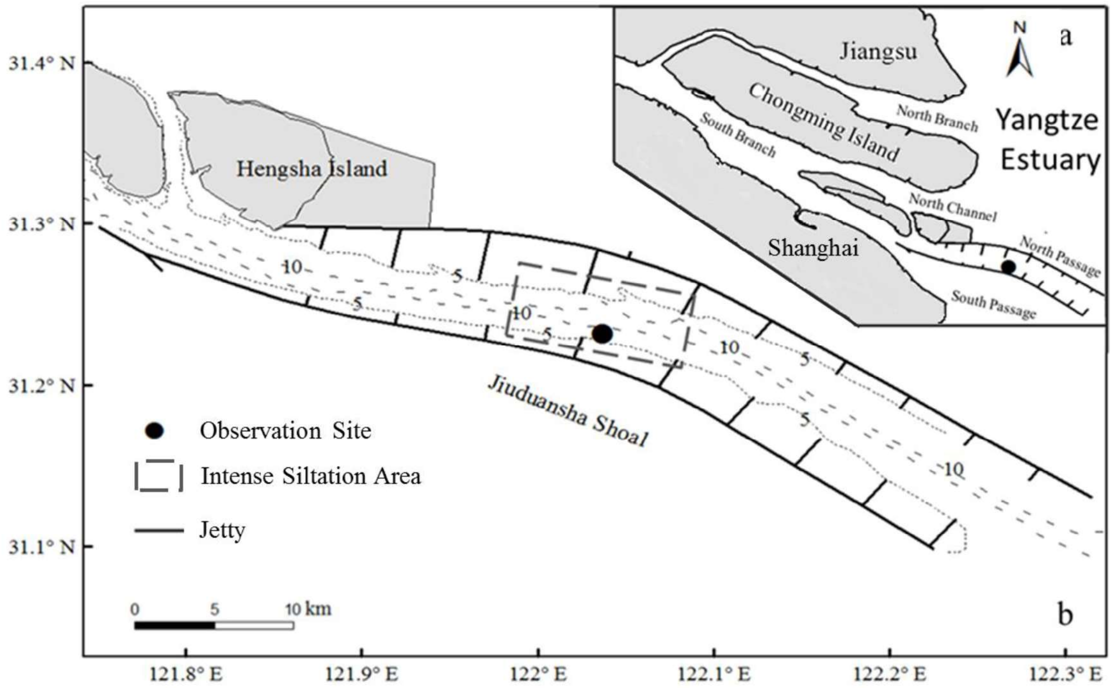

Fig. 1. Map of the morphology of the Yangtze estuary and the field observation site (black circle dot). Bathymetric contours of 5 and 10 shown are in meters referenced to the lowest low water.

2.2. In-situ measurements

Field works were conducted between July 13 and July 23 (wet season) in 2014, including spring, moderate, and neap tidal conditions. River discharges are about 46,000 m^3 s^{-1} at Datong during the field survey. A shipboard downward-looking ADCP (Acoustic Doppler Current Profilers) was used to measure current velocity. The sampling interval was 10 s and the bin size was 0.5 m. In-situ flocculated particle size distributions were measured with the LISST-100 (type C), and the range of particle size that the LISST-100C can differentiate is 2.5-500 μm with an accuracy of 1 phi. The LISST is based on light transmittance through a sample volume of water, it emits and records the laser in 32 scattering angle ranges, and then the signal is inverted to a volume distribution over 32 rings (Agrawal and Pottsmith, 2000). The LISST was lowered through the water column at a steady speed from 0.5 m below surface to 1 m above the bottom at a depth interval of about one-fifth of water depth every hour. LISST was set to sample every 5 seconds, and it measured at each layer (totally 6 layers) for at least 1 minute. A volume 1.2 liters of water sample was also collected every hour at 7 different water depths (0, 0.2, 0.4, 0.6, 0.8, 0.9 and 1.0 water depth) with an alpha water sampler, which was used for analyzing salinity, SSC, and primary particle size distribution.

Primary particle sizes were analyzed by a Coulter Counter after removing organic material and destroying flocs with sonification. By removing organic materials with hydrogen peroxide in lab, information of primary particles of both the macroflocs and microflocs could be obtained (Van Leussen, 1999). SSC were determined by filtration through pre-weighed filters, then the filters were dried at 60°C for eight hours. The organic matter contents of the sediment collected in spring and neap tide were determined through ignition at 450°C for 6 hours, results showed that organic matter in the mud of YE was about 3% (±1%).

2.3. Data processing

Floc properties

The LISST-100C recorded in-situ particle size distributions every 5 seconds, and then the raw data were analyzed by the LISST-SOP (version 5.00). The processed data were averaged over 1 min in each layer in order to eliminate short-term variations (Mikkelsen and Pejrup, 2001). The mean floc diameter D_M was calculated from the volume concentration distribution, and mean effective density of floc $\Delta\rho$ was calculated as below (Fettweis, 2008):

$$\Delta\rho = \rho_F - \rho_W = \frac{M_P}{V_F} - \rho_W = \left(1 - \frac{\rho_W}{\rho_P}\right)\frac{M_P}{V_F} \quad (1)$$

where ρ_F is floc density, ρ_W is water density, V_F is the floc volume concentration derived from LISST and M_P indicates the mass suspended sediment concentration measured through filtration of water samples. ρ_P is primary particle density which is estimated to be 2,570 kg m^{-3}, given a density of 1,300 kg m^{-3} for organic matter (Markussen and Andersen, 2013) and an organic matter content of 3% (mass ratio) determined by loss on ignition. The effective densities of flocs are used here to indicate the ability of the flocs being suspended in the water in counteracting the buoyancy.

Based on the self-similar fractal entities, it was proposed by Kranenburg (1994) that:

$$\Delta\rho \propto (\rho_P - \rho_W)(\frac{D_M}{d})^{nf-3} \quad (2)$$

where d is the diameter of the primary particle and nf is the floc fractal dimension, a mathematical parameter used as an indicator of particle morphology. The fractal dimension of flocs usually varies between about 1.4 for large fragile flocs, and about 2.2 for strong flocs (Kranenburg, 1994).

During this investigation, all the mean floc diameters were smaller than 100 μm, thus the Stokes' formula was used to estimate settling velocity as follows:

$$\omega_s = \frac{{D_M}^2 \Delta\rho g}{18\mu} \quad (3)$$

where g is the acceleration due to gravity and μ is the molecular viscosity of water.

Turbulent shear

The shear rate parameter G in the logarithmic velocity layer was calculated in accordance with Pejrup and Mikkelsen (2010):

$$G = \sqrt{\frac{u_*^3(1-z/H)}{\nu\kappa z}} \quad (4)$$

where v is the kinematic viscosity, κ is Von Karman's constant (κ=0.41), z is the height above bed, H is the water depth and u_* is the friction velocity, it can be calculated through:

$$u_* = \frac{u_b\kappa}{ln\,(z/z_0)} \quad (5)$$

u_b is the current velocity, z_0 is the roughness length, and z_0 is assumed to be constant of 3 mm in this work. This value has been used in the simulation of sediment transport in the turbidity maxima of the YE (Ge et al., 2012).

3. Results

3.1. Hydrodynamics and sediment concentrations

Figure 2 shows vertically and time varying mean flow velocity, near bottom turbulence, salinity, SSC, and mean floc size at spring and neap tides.

During the field survey period, there were no strong winds, so the influence of wind and wind-generated waves can be ignored. Turbulent shear in the water was mainly caused by flow velocity and varied with tidal phases.

The time series of current velocities suggested that tidal waves were asymmetrical with an ebb-dominance, the maximum vertically-averaged ebb flow velocities were 2.3 m s^{-1} and 1.4 m s^{-1} at spring and neap tides, respectively (Figures 2a, and 2e). During flood period, acceleration and deceleration stages were also asymmetrical. It only took about 2 hours from low water slack (LWS) to maximum flood, which was one half of the decelerating time. However, the time of accelerating and decelerating during ebb was almost the same.

Vertical variations of salinity and SSC over time are presented also in Figure 2. Salinity was lower than 2‰ most of the time, and the maximum salinity was about 11‰ at both spring and neap tides. Large salinity only lasted a few hours around high water slack (HWS). At spring tide, the smallest SSC through the water column was about 0.1 g l^{-1} and SSC was larger than 0.3 g l^{-1} most of the time. The mean SSC was 0.68±0.28 g l^{-1} and there were four peaks of SSC during the investigation period of two tidal cycles. Increased current velocity led to high near-bed turbulent shears and resulted in sediment resuspension around the peak flood periods. During the shift from flood to ebb, the near bottom SSC increased fast, and the largest SSC reached 7 g l^{-1}. High SSC in the surface of water column dropped rapidly around HWS which can be attributed to flocculation-enhanced settling. At neap tide, SSC became smaller compared to spring tide. The maximum bottom SSC was 1.73 g l^{-1} and the averaged SSC over the whole tidal cycle was 0.24±0.12 g l^{-1}. Overall SSC increased with increased bottom shear stress.

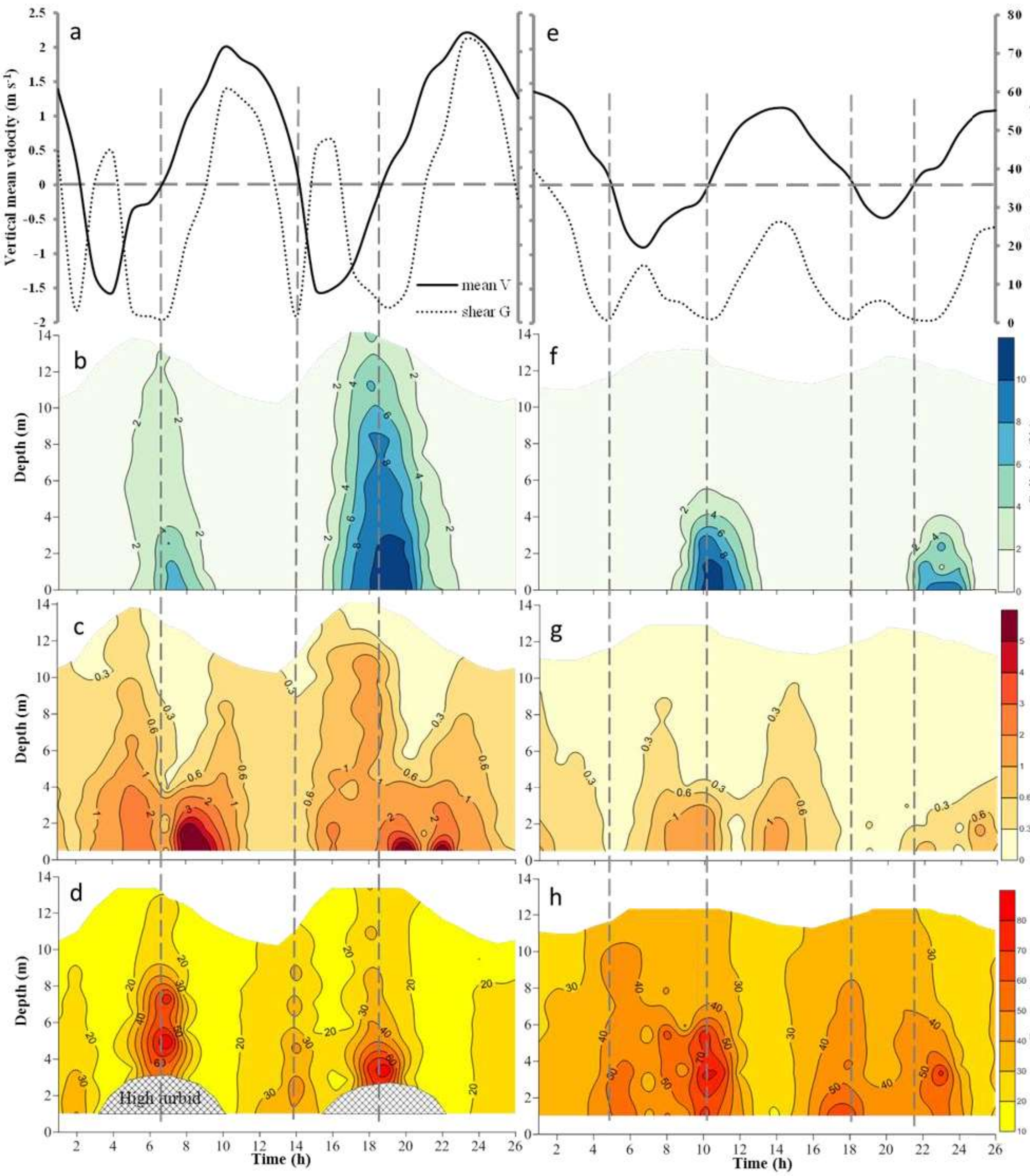

Fig. 2. (a, e) Vertical mean flow velocity and turbulent shear (ebb is positive), (b, f) salinity in ‰, (c, g) suspended sediment concentration in g l^{-1}, and (d, h) distribution of mean floc size in μm. Left panels are results at spring tide, and right four panels are the results at neap tide.

3.2. Floc parameters

Mean floc diameter

The D_M varied between 14 and 95 μm in a tidal cycle at spring tide with a mean value of 27±13 μm (Figure 2d). The mean D_M was 43±10 μm at neap tide, about 57% larger than spring tide. Floc sizes varied largely in a tidal cycle. Larger flocs developed around slack waters of low turbulent intensity, and flocs were larger during HWS than LWS. It was found that the largest flocs systematically occurred with the peaks of salinity around HWS. Floc size increased from surface to near bottom during slack water, though, part of the near bottom data were not obtained as a result of too high turbidity for LISST to work normally. Smaller flocs persisted at time with strong turbulence, particularly around peak flood and ebb tides.

Vertical distribution and particle size distribution (PSD)

Figures 3a, and 3b show vertical profiles of mean floc sizes during different typical tidal phases at spring tide. Flocs were smallest in size when current magnitudes were maximal and flocs at different depths were larger during the slack water period. D_M was uniform at all depths at both flood and ebb acceleration and peak velocity periods. However, D_M increased from surface layer to near bottom layer during the time of deceleration and slack waters, which can be ascribed to differential settling when the turbulent shear was low.

Figures 3c and 3d show PSDs of in-situ flocs at peak flood and LWS and the averaged PSD of primary particles. The PSD of primary particles is unimodal with a peak at about 10 μm, but that of in-situ flocs detected by LISST are mainly bimodal. One peak of the floc PSD corresponds to 10 μm as the PSD of primary particles, whereas the second peak of floc PSD around 30-90 μm is more prominent. The larger peak at LWS increased from surface to bottom layers, the same tendency as D_M profile. Note that there were raised tails at both ends of the distribution curves, because of the presence of flocs beyond the confined measurement range (2.5-500 μm) of LISST. These flocs with diameter <2.5 μm and >500 μm are likely to cause over- or under-estimation of D_M to some degree, respectively. Voulgaris and Meyers (2004) tried to minimize this effect by creating additional rings corresponding to larger size bands, and it turned out that this measure did not cause a big difference because the dominant portion of flocs are detected by LISST. For that reason, the impact of the tails on the PSD of flocs was not treated.

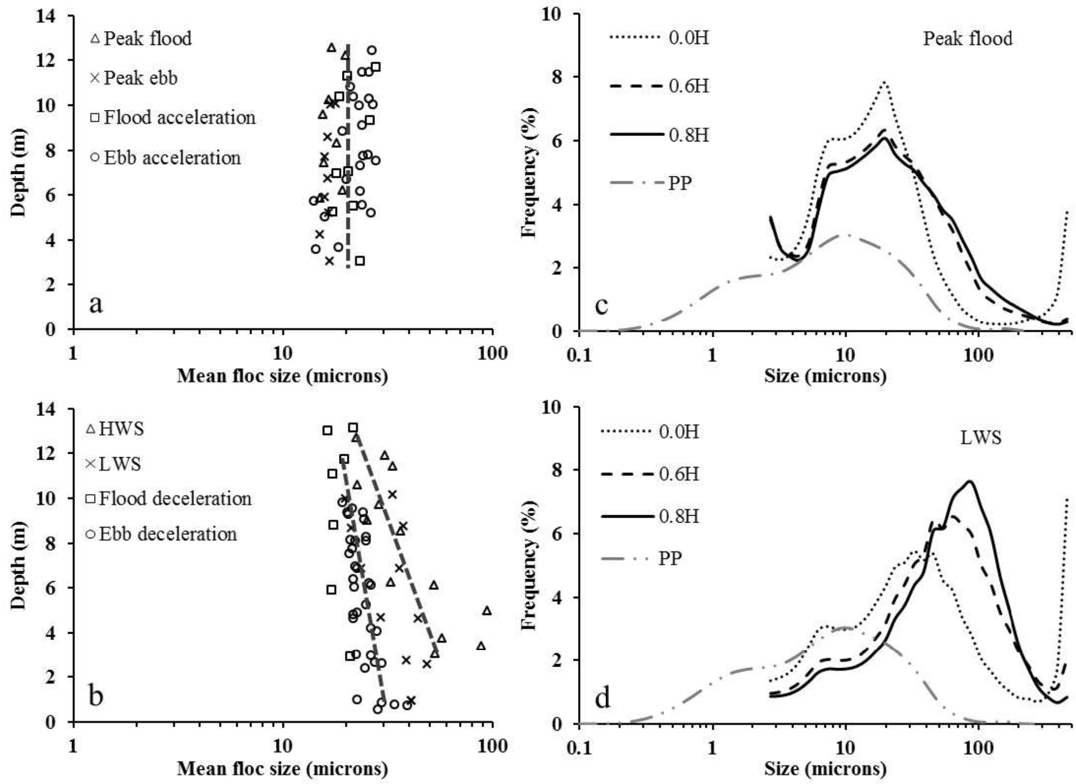

Fig. 3. Panels (a) and (b) show vertical variations of mean floc size in different tidal phases, and panels (c) and (d) show size distributions of both dispersed and flocculated particles. Panel (c) shows the results at peak flood and (d) shows the results at LWS at spring tide. PP indicates primary particle, and H is the water depth.

Effective density and settling velocity of flocs

The effective density of flocs calculated by equation (1) varied between 60 and 450 kg m^{-3}. It tended to decrease with increasing floc size and the mean effective density of all the flocs observed was 215 kg m^{-3} (Figure 4). However, there was a wide scattering of effective density for a certain D_M. Most of the floc size was in the range of 30-60 μm, and the largest spread of effective density also occurred in this range, indicating that the effective densities of flocs with the same D_M might change significantly due to various floc structures. The fractal dimension nf was estimated to be in the range of 1.5-2.1, and the best fit is nf=1.8 in this field survey (see Figure 4). An fractal dimension of 1.8 was smaller than the average nf=2 concluded by Winterwerp (1998) through published researches in the Ems Estuary, the North Sea (van Leussen, 1994), and the Tamar Estuary (Fennessy et al., 1994a), indicating that flocs in the YE might be more fragile.

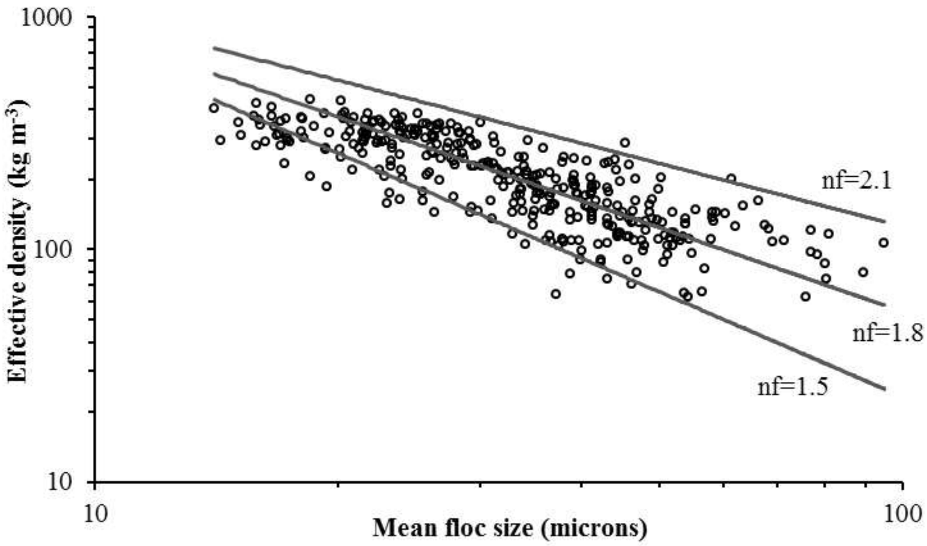

Fig. 4. Variations of effective density with mean floc size.

Settling velocities of flocs varied between 0.04 and 0.6 mm s^{-1} in this study, and it increased with increasing D_M (see Figure 5). Most of the settling velocities were in the range of 0.08-0.3 mm s^{-1}. Note that the same floc size group might have settling velocities varying in a big range, and on the other hand flocs of varying sizes may have the same settling velocity due to the difference in floc structure and density. It was found that most of the large settling velocities occurred at water slack periods, which were marked as red circles in Figure 5. The averaged settling velocity at water slack periods was 0.2 mm s^{-1}, which was 67% larger than the averaged result of 0.12 mm s^{-1} in the other time. Shi et al. (2003) calculated settling velocities of 0.4-4.1 mm s^{-1} based on Rouse SSC profiles in the YE. But vertical SSC profiles have many kinds of patterns as a result of the complex hydrodynamics in estuaries, thus the Rouse SSC profile is not representative in a tidal system. The research of Shao et al. (2010) showed that high sediment concentrations caused by resuspension will mislead to greater settling velocity through Rouse equation, and this may be the reason that the smallest and largest settling velocity calculated by Shi et al. (2003) was much larger than the estimation in this study (0.04 mm s^{-1} and 0.6 mm s^{-1}, respectively).

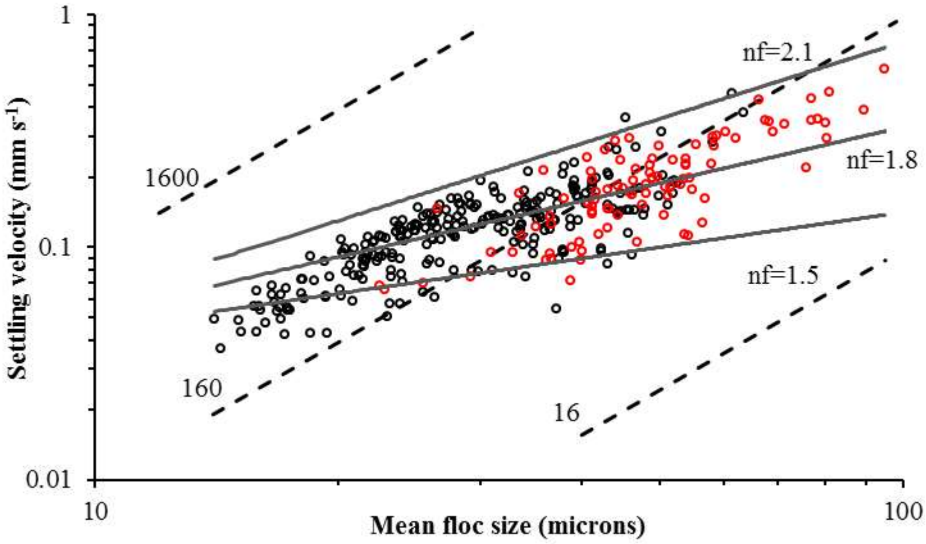

Fig. 5. Variations of settling velocities of flocs with D_M. Red and black circles were results at water slack periods and other time, respectively. Dashed lines of 1,600, 160 and 16 represent the effective density isolines of spherical quartz particles, the unit is kg m^{-3}, and grey lines show the relationships of settling speed and size under different floc fractal dimensions.

4. Discussion

4.1. Flocculation processes

It is known that transportation of suspended cohesive sediment is mainly driven by the cycle of suspension, flocculation, settling, deposition, erosion, and resuspension (Eisma, 2012). Flocculation process plays a key role in this cycle as it can affect the size and density of suspended particles, and control the settling velocity of sediment. Meanwhile, heavy mental, contaminants, and pollutants can easily adhere to flocs, thus the fate and transport of flocs could also have great effects in biochemical matter transport.

Large flocs or macroflocs (>125 um, Eisma, 1986) have a larger diameter and smaller density, and potentially larger settling velocity, thus tend to account for most of the vertical settling flux (Fennessy et al., 1997; Manning and Dyer, 2007). On the other hand, the large flocs are more fragile, less denser and can be easily broken down into smaller ones. On the contrary, smaller flocs or microflocs (<125 um) usually have a denser structure, higher density, and are more resilient to turbulent breaking force, and they have a high potential to aggregate again to form larger flocs (Dyer and Manning, 1999).

Data collected in this field survey revealed floc dynamic variations within a tidal cycle and the spring-neap cycle. The variances of mean floc size through the water column shown in Figures 2d and 2h indicated active flocculation and break-up processes in the YE. The D_M ranged between 14-95 μm and 20-80 μm during spring tide and neap tide, respectively. However, the variations of primary particle size were much more limited, with median size around 6-8 μm. Meanwhile, the bimodal PSDs of flocs (see Figures 3c and 3d) with a small peak at around 10 μm similar to that of primary particles indicated that a part of inert particles are still disaggregated in the natural environments, and other parts of primary populations flocculated and formed a more significant larger peak, varying from 30 to 90 μm.

Within a tidal cycle, it was found that large flocs occurred systematically around slack water at both spring and neap tides, and the averaged floc size around water slack was 45±20 μm at spring tide. However, it was only 22±5 μm at other tidal phases. Between spring-neap tidal cycles, although the maximal floc size observed at spring tide was a little larger, the averaged floc size during neap tidal cycles was 57% larger.

During slack waters, it was interesting to find that flocs tended to develop from surface to bottom (Figure 3b), suggesting that differential settling could dominate the flocculation process during these low shear stress periods (Chen et al., 1994; Fugate and Friedrichs, 2003). Laboratory experiments with sediment samples of a mud content of 70% by Wendling et al. (2015) exhibited that settling velocity at the bottom of the settling column was 20 times larger than that at surface, also indicating significant flocculation occurred during settling in still water.

4.2.Controls on in-situ flocculation

Effects of Turbulent Shear

Among many influential factors, turbulence is thought to be the controlling factor determining maximum floc sizes in tidal cycles (Winterwerp, 1998; Dyer and Manning, 1999). It is also widely known that there is a critical shear stress beneficial to flocculation mostly. Below this threshold, an increase in turbulence strength would increase the collision frequency of particles, thus leading to stronger aggregation. Increase of turbulence strength beyond the threshold would break up fragile flocs (Eisma, 1986; Manning and Dyer, 1999; Winterwerp, 2002), and resulting in floc disruption. The critical shear stress was found in many published works, including laboratory experiments by Manning and Dyer (1999) and field study by Sahin (2014) and Markussen and Andersen (2014), and in their researches, a critical shear value of 0.35 N m^{-2} (G≈27 s^{-1}), G≈20 s^{-1}, and G of about 4 s^{-1} was obtained, respectively, suggesting a big range of variations.

In this study, Figure 6 shows the relationship between D_M and turbulent dissipation parameter G. The regression of our field data did not quantify critical shear well, and an overall negative relationship between D_M and G was got, with the regression parameter R^2=0.64. A plateau of floc size for G values <3 s^{-1} was identified, and when turbulent shear became larger than 3 s^{-1}, D_M decreased significantly with the increasing G, once turbulent shear G exceeded 40-50 s^{-1}, D_M through water column were only about 20 μm, suggesting that almost all flocs excepted the strongest small ones broke up under high turbulent shear.

The largest vertically-averaged D_M of flocs is about 70 μm in the present work, which is much smaller than many other field observations conducted in less turbid estuaries (Eisma and Li, 1993; Curran et al., 2007; Wang et al., 2013). As we know, floc size is the result of dynamic equilibrium between flocculation and break-up processes, and biological factors could mediate both processes. On one hand, the organic material can adhere to primary particles, change their surface charge, and increase the probability of cohesion after collision (Mietta et al., 2009). On the other hand, Winterwerp and van Kesteren (2004) showed that many organic matters contain long polymers, which might connect different particles through 'bridging'. Thus the increasing of organic matter could increase turbulent shear threshold in breaking flocs. In this study, low content of organic matter about 3% in the high turbid YE might contribute to the overall small flocs compared to other systems.

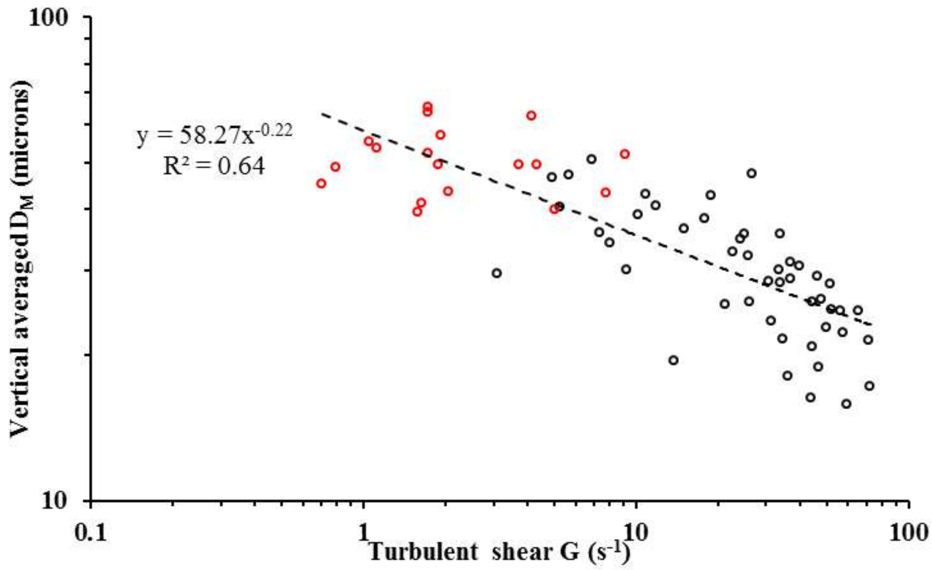

Fig. 6. Variations of vertical averaged D_M with turbulent shear. Red and black circles are results at water slack periods and other time, respectively.

Impacts of SSC

Increasing SSC within a range will lead to increased particle collision frequency and enhance floc growth (Eisma and Li, 1993; van der Lee, 2000). However, the effects of SSC on flocculation were found insignificant in some lab and field work (Milligan and Hill, 1998; Xia et al., 2004). Moreover, Burban et al. (1989) found that median floc size decreased as the SSC increased in their experiments. Note that these observations were confined to environments with SSC around 0.05-0.25 g l^{-1}, which was smaller than the typical turbidity range in this study, i.e., 0.05-1.1 g l^{-1}. A wide scatter of D_M corresponds to SSC was shown in Figure 7. Floc size tended to increase with increasing SSC at water slack periods and a negative relationship was found in other tidal periods. However, it is noticed that both the correlations are poor (R^2=0.23 and R^2=0.08, respectively). We think that the highly variable estuarine environments might lead to the opposite tendency and poor correlations between floc size and SSC. As flocculation is influenced by both physical and biochemical processes, and many factors that have effects on the processes can be dependent on each other and change simultaneously (e.g., turbulence, SSC, salinity, and organic matter). Moreover, SSC is related to the resuspension process, which plays an important role in determining near bottom floc size distributions (Fugate and Friedrichs, 2003).

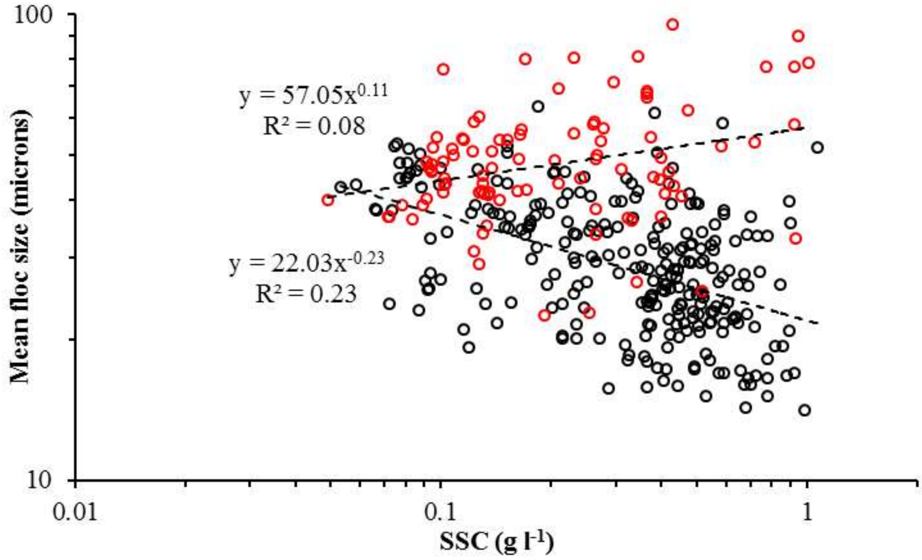

Fig. 7. Variations of mean floc size with SSC. Red and black circles are results at water slack periods and other time, respectively.

4.3. Implications for siltation

Floc settling velocity and SSC both varied significantly in a tidal cycle. The largest settling velocity occurred around HWS in the NP, and it was found that SSC decreased sharply after HWS at spring tide (see Figure 2c). The rapid decreasing of SSC was mainly caused by fast settling of large flocs that developed during low turbulence intensity. We estimated vertical settling flux by multiplying SSC and settling velocity of flocs. At neap tide, the time varying settling flux ranged between 0.01-0.07 g m^{-2} s^{-1}, and the averaged settling flux was 0.032 g m^{-2} s^{-1} (Figure 8). The averaged value at spring tide was 0.066 g m^{-2} s^{-1}, and the settling fluxes at HWS and LWS at spring tide were about 0.3 and 0.1 g m^{-2} s^{-1}, respectively, which was a few times larger than the settling fluxes in the other periods. The fast settling speed of large flocs especially around HSW together with high SSC through water column resulted in huge settling flux around high water. Uncles et al. (2010) observed similar phenomenon in the Tamar Estuary that a rapid reduction of SSC on flood tides within 2.5 h of HW. Moreover, the upward flux around HW was small, indicating that the settling of large flocs around HW played a controlling role in the deposition of suspended sediment. And after the fast settling of particles at HWS, large amounts of sediment are confined predominantly within the bottom layer, thus they will not be easily transported seaward in the following ebb period. These would lead to rapid accumulation of sediment in the study area.

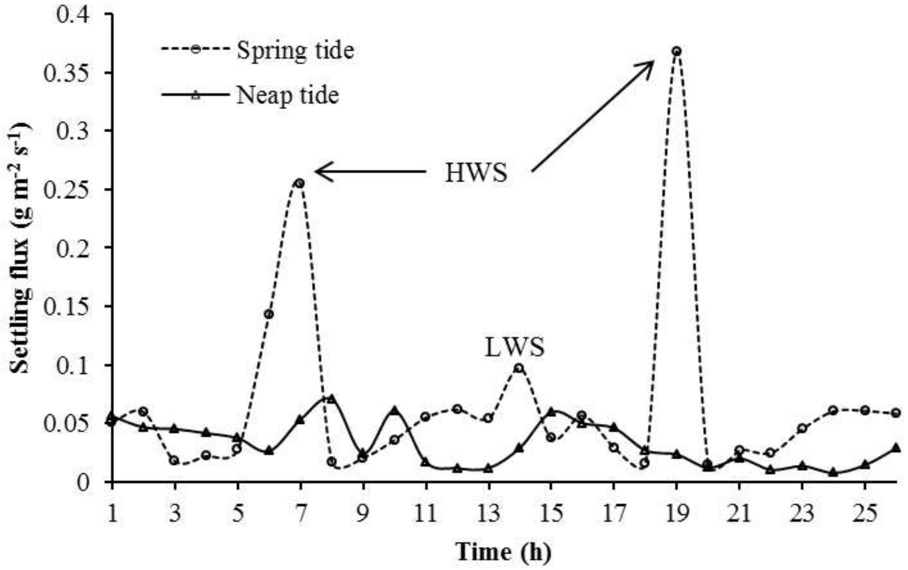

Fig. 8. Time varying settling fluxes of sediment at spring and neap tides.

5. Conclusions

This study examined in-situ flocculation dynamics based on data of current and sediment properties in the TM of the YE. Floc diameter was measured by a LISST-100C, and settling velocity was estimated based on floc size and effective density.

Mean floc diameters varied between 14-95 μm and flocculation exhibited strong temporal and vertical variations within a tidal cycle and between spring-neap cycles. Large flocs occurred systematically around slack waters and floc sizes increased from surface to bottom during the deceleration and slack water periods. The averaged floc size at neap tide was 57% larger than at spring tide. Effective density of flocs decreased with the increase of floc size, and fractal dimension of floc in the YE was mainly between 1.5 and 2.1.

Turbulent shear plays a dominant role in controlling processes of flocs aggregation and break-up. Floc size decreased significantly with the increase of turbulent shear when turbulent shear was beyond the range of 2-3 s^{-1}. Correlations between SSC and floc size was poor suggesting SSC is not significant in controlling flocculation in this study based on the field data.

Settling velocity of flocs ranged between 0.04-0.6 mm s^{-1} and it changed in different tidal phases. The largest settling flux happened at the HWS during spring tide, which was caused by fast settling of large flocs together with high SSC. This mechanism might be an important factor leading to rapid accumulation of sediment at the study area where serious back-siltation happened during the wet season. Future work is needed to examine the flocculation sensitivity to the physical parameters in a more quantified manner with laboratory experiments.

Acknowledgements

The study is funded by the National Natural Science Foundation of China (NSFC) (No. 51320105005, 41276080, 41506105) and SKLEC-fund (No. 2015RCDW02). The comments and suggestions from two anonymous reviewers and the associate editor Andrew J. Manning are greatly appreciated.

References

Agrawal, Y.C., Pottsmith, H.C., 2000. Instruments for particle size and settling velocity observations in sediment transport. Mar. Geol. 168, 89–114. doi:10.1016/S0025-3227(00)00044-X

Burban, P.Y., Lick, W., Lick, J., 1989. The flocculation of fine-grained sediments in estuarine waters. J. Geophys. Res. 94, 8323–8330. doi:10.1029/JC094iC06p08323

Chen, S., Eisma, D., Kalf, J., 1994. In situ distribution of suspended matter during the tidal cycle in the elbe estuary. Netherlands J. Sea Res. 32, 37–48. doi:10.1016/0077-7579(94)90026-4

Curran, K.J., Hill, P.S., Milligan, T.G., Mikkelsen, O.A., Law, B.A., Durrieu de Madron, X., Bourrin, F., 2007. Settling velocity, effective density, and mass composition of suspended sediment in a coastal bottom boundary layer, Gulf of Lions, France. Cont. Shelf Res. 27, 1408–1421. doi:10.1016/j.csr.2007.01.014

Droppo, I.G., Ongley, E.D., 1992. The state of suspended sediment in the freshwater fluvial environment: a method of analysis. Water Res. 26, 65–72.

Dyer, K.R., 1989. Sediment processes in estuaries: Future research requirements. J. Geophys. Res. 94, 14327–14339. doi:10.1029/JC094iC10p14327

Dyer, K.R., Manning, A.J., 1999. Observation of the size, settling velocity and

effective density of flocs, and their fractal dimensions. J. Sea Res. 41, 87–95.
Eisma, D., 2012. Suspended matter in the aquatic environment. Springer Science & Business Media.
Eisma, D., 1986. Flocculation and de-flocculation of suspended matter in estuaries. Netherlands J. Sea Res. 20, 183–199. doi:10.1016/0077-7579(86)90041-4
Eisma, D., Li, A., 1993. Changes in suspended-matter floc size during the tidal cycle in the Dollard estuary. Netherlands J. Sea Res. 31, 107–117.
Eisma, D., Schuhmacher, T., Boekel, H., Van Heerwaarden, J., Franken, H., Laan, M., Vaars, A., Eijgenraam, F., Kalf, J., 1990. A camera and image-analysis system for in situ observation of flocs in natural waters. Netherlands J. Sea Res. 27, 43–56. doi:10.1016/0077-7579(90)90033-D
Fennessy, M.J., Dyer, K.R., Huntley, D.A., 1994a. inssev: An instrument to measure the size and settling velocity of flocs in situ. Mar. Geol. 117, 107–117. doi:10.1016/0025-3227(94)90009-4
Fennessy, M.J., Dyer, K.R., Huntley, D.A., 1994b. Size and settling velocity distributions of flocs in the Tamar Estuary during a tidal cycle. Aquat. Ecol. 28, 275–282.
Fennessy, M.J., Dyer, K.R., Huntley, D.A., Bale, A.J., 1997. Estimation of settling flux spectra in estuaries using INSSEV, in: Cohesive Sediments—proc. of INTERCOH Conf. Wiley, Chichester. pp. 87–104.
Fettweis, M., 2008. Uncertainty of excess density and settling velocity of mud flocs derived from in situ measurements. Estuar. Coast. Shelf Sci. 78, 426–436. doi:10.1016/j.ecss.2008.01.007
Fugate, D.C., Friedrichs, C.T., 2003. Controls on suspended aggregate size in partially mixed estuaries. Estuar. Coast. Shelf Sci. 58, 389–404. doi:10.1016/S0272-7714(03)00107-0
Fugate, D.C., Friedrichs, C.T., 2002. Determining concentration and fall velocity of estuarine particle populations using ADV, OBS and LISST. Cont. Shelf Res. 22, 1867–1886.
Ge, J., Chen, C., Qi, J., Ding, P., Beardsley, R.C., 2012. A dike–groyne algorithm in a terrain-following coordinate ocean model (FVCOM): Development, validation and application. Ocean Model. 47, 26–40.
Guan, X., Chen, Y., Du, X., 1996. Experimental study on mechanism of flocculation in Yangtze Estuary (in Chinese). J. Hydraul. Eng. 6, 70–80.
Guo, L., He, Q., 2011. Freshwater flocculation of suspended sediments in the Yangtze River, China. Ocean Dyn. 61, 371–386.
Jiang, G., Yao, Y., Tang, Z., 2002. Analysis of influencing factors on fine sediment flocculation in the Changjiang Estuary (in Chinese). Acta Oceanol. Sin. 21, 385–394.
Kranenburg, C., 1994. The fractal structure of cohesive sediment aggregates. Estuar. Coast. Shelf Sci. 39, 451–460. doi:10.1016/S0272-7714(06)80002-8
Manning, A.J., 2004. Observations of the properties of flocculated cohesive sediment in three western European estuaries. J. Coast. Res. 70–81.
Manning, A.J., Dyer, K.R., 2007. Mass settling flux of fine sediments in Northern

European estuaries: Measurements and predictions. Mar. Geol. 245, 107–122. doi:10.1016/j.margeo.2007.07.005

Manning, A.J., Dyer, K.R., 1999. A laboratory examination of floc characteristics with regard to turbulent shearing. Mar. Geol. 160, 147–170. doi:10.1016/S0025-3227(99)00013-4

Markussen, T.N., Andersen, T.J., 2014. Flocculation and floc break-up related to tidally induced turbulent shear in a low-turbidity, microtidal estuary. J. Sea Res. 89, 1–11.

Markussen, T.N., Andersen, T.J., 2013. A simple method for calculating in situ floc settling velocities based on effective density functions. Mar. Geol. 344, 10–18. doi:10.1016/j.margeo.2013.07.002

McCave, I.N., 1984. Size spectra and aggregation of suspended particles in the deep ocean. Deep Sea Res. Part A, Oceanogr. Res. Pap. 31, 329–352. doi:10.1016/0198-0149(84)90088-8

Mehta, A.J., 2013. An introduction to hydraulics of fine sediment transport. World Scientific Publishing Co Inc.

Mietta, F., Chassagne, C., Manning, A.J., Winterwerp, J.C., 2009. Influence of shear rate, organic matter content, pH and salinity on mud flocculation. Ocean Dyn. 59, 751–763. doi:10.1007/s10236-009-0231-4

Mikkelsen, O., Pejrup, M., 2001. The use of a LISST-100 laser particle sizer for in-situ estimates of floc size, density and settling velocity. Geo-Marine Lett. 20, 187–195.

Milligan, T.G., Hill, P.S., 1998. A laboratory assessment of the relative importance of turbulence, particle composition, and concentration in limiting maximal floc size and settling behaviour. J. Sea Res. 39, 227–241.

Partheniades, E., 1993. Turbulence, flocculation and cohesive sediment dynamics. Nearshore Estuar. cohesive sediment Transp. 40–59.

Pejrup, M., Mikkelsen, O.A., 2010. Factors controlling the field settling velocity of cohesive sediment in estuaries. Estuar. Coast. Shelf Sci. 87, 177–185. doi:10.1016/j.ecss.2009.09.028

Sahin, C., 2014. Investigation of the variability of floc sizes on the Louisiana Shelf using acoustic estimates of cohesive sediment properties. Mar. Geol. 353, 55–64.

Shao, Y., Yan, Y., Maa, J.P.-Y., 2010. In situ measurements of settling velocity near Baimao shoal in Changjiang estuary. J. Hydraul. Eng. 137, 372–380.

Shi, Z., Zhou, H.J., Eittreim, S.L., Winterwerp, J.C., 2003. Settling velocities of fine suspended particles in the Changjiang Estuary, China. J. Asian Earth Sci. 22, 245–251. doi:10.1016/S1367-9120(03)00067-1

Song, D., Wang, X.H., 2013. Suspended sediment transport in the Deepwater Navigation Channel, Yangtze River Estuary, China, in the dry season 2009: 2. Numerical simulations. J. Geophys. Res. Ocean. 118, 5568–5590. doi:10.1002/jgrc.20411

Soulsby, R.L., Manning, A.J., Spearman, J., Whitehouse, R.J.S., 2013. Settling velocity and mass settling flux of flocculated estuarine sediments. Mar. Geol. 339, 1–12. doi:10.1016/j.margeo.2013.04.006

Stolzenbach, K.D., Elimelech, M., 1994. The effect of particle density on collisions between sinking particles: implications for particle aggregation in the ocean. Deep. Res. Part I 41, 469–483. doi:10.1016/0967-0637(94)90091-4

Tang, J.H., 2007. Characteristics of fine cohesive sediment's flocculation in the Changjiang estuary and its adjacent sea area. Master Degree thesis, East China Norm. Univ. May.

Tsai, C.H., Iacobellis, S., Lick, W., 1987. Flocculation of Fine-Grained Lake Sediments Due to a Uniform Shear Stress. J. Great Lakes Res. 13, 135–146. doi:10.1016/S0380-1330(87)71637-2

Uncles, R.J., Bale, A.J., Stephens, J.A., Frickers, P.E., Harris, C., 2010. Observations of floc sizes in a muddy estuary. Estuar. Coast. Shelf Sci. 87, 186–196.

van der Lee, W.T.B., 2000. Temporal variation of floc size and settling velocity in the Dollard estuary. Cont. Shelf Res. 20, 1495–1511. doi:10.1016/S0278-4343(00)00034-0

van Leussen, W., 1994. Estuarine macroflocs and their role in fine-grained sediment transport. Ministry of Transport, Public Works and Water Management, National Institute for Coastal and Marine Management (RIKZ).

van Leussen, W., 1999. The variability of settling velocities of suspended fine-grained sediment in the Ems estuary, in: Journal of Sea Research. pp. 109–118. doi:10.1016/S1385-1101(98)00046-X

Voulgaris, G., Meyers, S.T., 2004. Temporal variability of hydrodynamics, sediment concentration and sediment settling velocity in a tidal creek. Cont. Shelf Res. 24, 1659–1683. doi:10.1016/j.csr.2004.05.006

Wan, Y., Wu, H., Roelvink, D., Gu, F., 2015. Experimental study on fall velocity of fine sediment in the Yangtze Estuary, China. Ocean Eng. 103, 180–187.

Wang, Y.P., Voulgaris, G., Li, Y., Yang, Y., Gao, J., Chen, J., Gao, S., 2013. Sediment resuspension, flocculation, and settling in a macrotidal estuary. J. Geophys. Res. Ocean. 118, 5591–5608.

Wendling, V., Gratiot, N., Legout, C., Droppo, I.G., Coulaud, C., Mercier, B., 2015. Using an optical settling column to assess suspension characteristics within the free, flocculation, and hindered settling regimes. J. Soils Sediments 15, 1991–2003.

Whitehouse, R.J.S., Soulsby, R.L., Roberts, W., Mitchener, H.J., 2000. Dynamics of estuarine muds: a manual for practical applications., Dynamics of estuarine muds: a manual for practical applications. Report SR 527.

Winterwerp, J.C., 2002. On the flocculation and settling velocity of estuarine mud. Cont. Shelf Res. 22, 1339–1360. doi:10.1016/S0278-4343(02)00010-9

Winterwerp, J.C., 1998. A simple model for turbulence induced flocculation of cohesive sediment. J. Hydraul. Res. 36, 309–326.

Winterwerp, J.C., Van Kesteren, W.G.M., 2004. Introduction to the physics of cohesive sediment dynamics in the marine environment. Elsevier.

Xia, X.M., Li, Y., Yang, H., Wu, C.Y., Sing, T.H., Pong, H.K., 2004. Observations on the size and settling velocity distributions of suspended sediment in the Pearl River Estuary, China. Cont. Shelf Res. 24, 1809–1826.

doi:10.1016/j.csr.2004.06.009
Xie, R., Wu, D.A., Yan, Y., Zhou, H., 2010. Fine silt particle pathline of dredging sediment in the Yangtze River deepwater navigation channel based on EFDC model. J. Hydrodyn. Ser. B 22, 760–772.
Zhang, Z., Ruan, W., Jiang, G., 1995. The relationship between floc settlement in flowing water and deposition in the Changjiang estuary mouth bar area (in Chinese). Oceanol. Limnol. Sin. 378–383.

Click here to download high resolution image

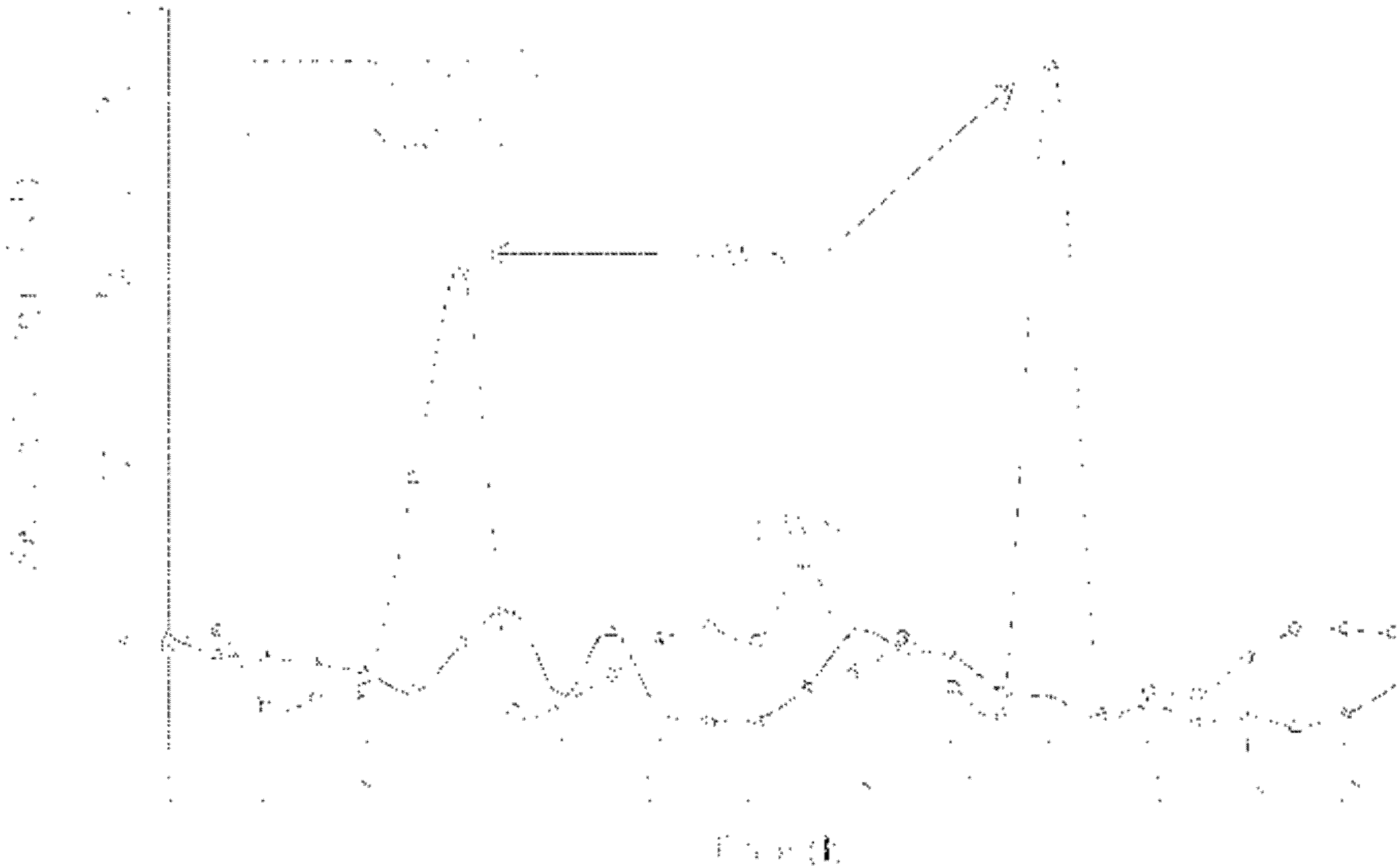

Click here to download high resolution image

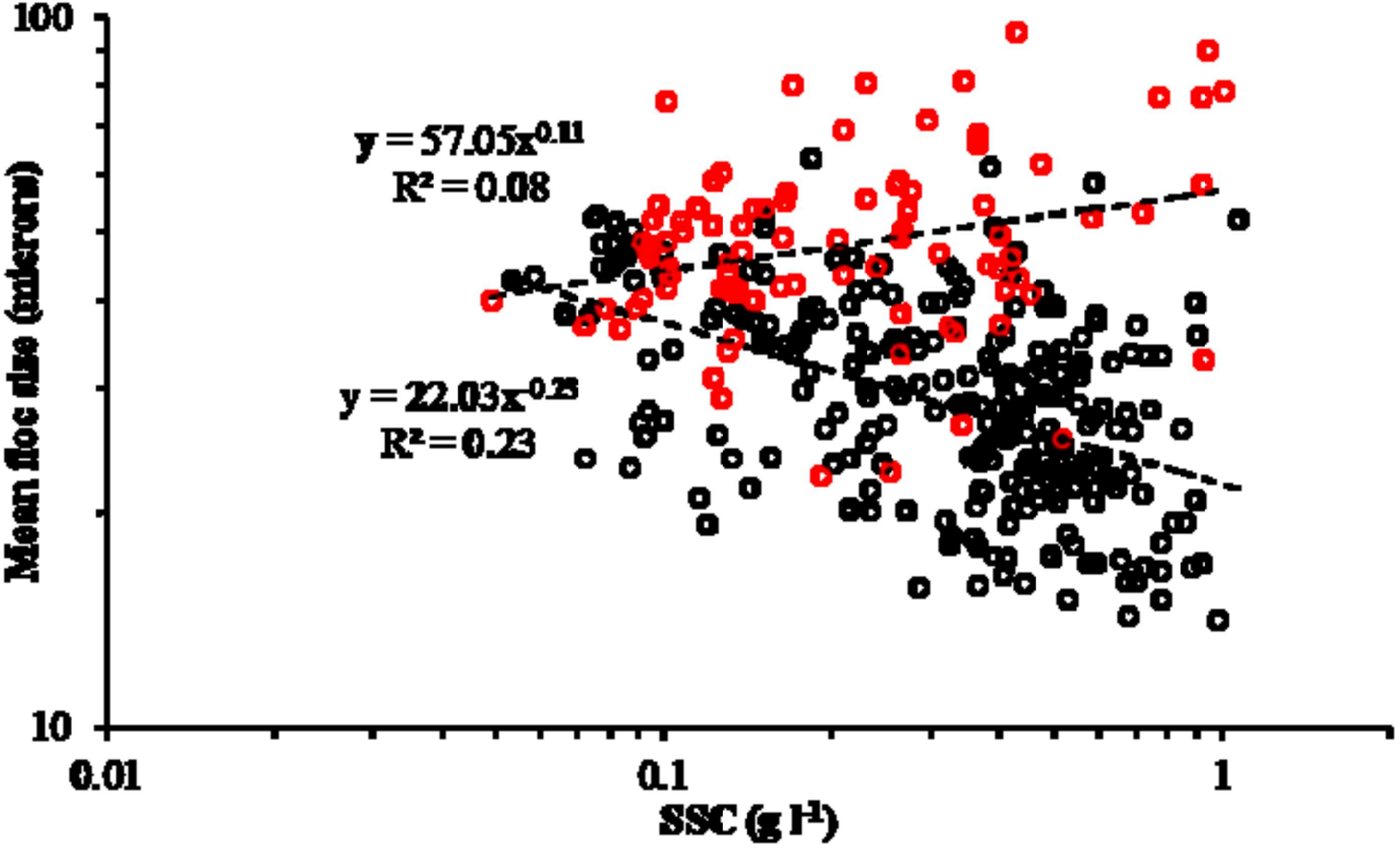

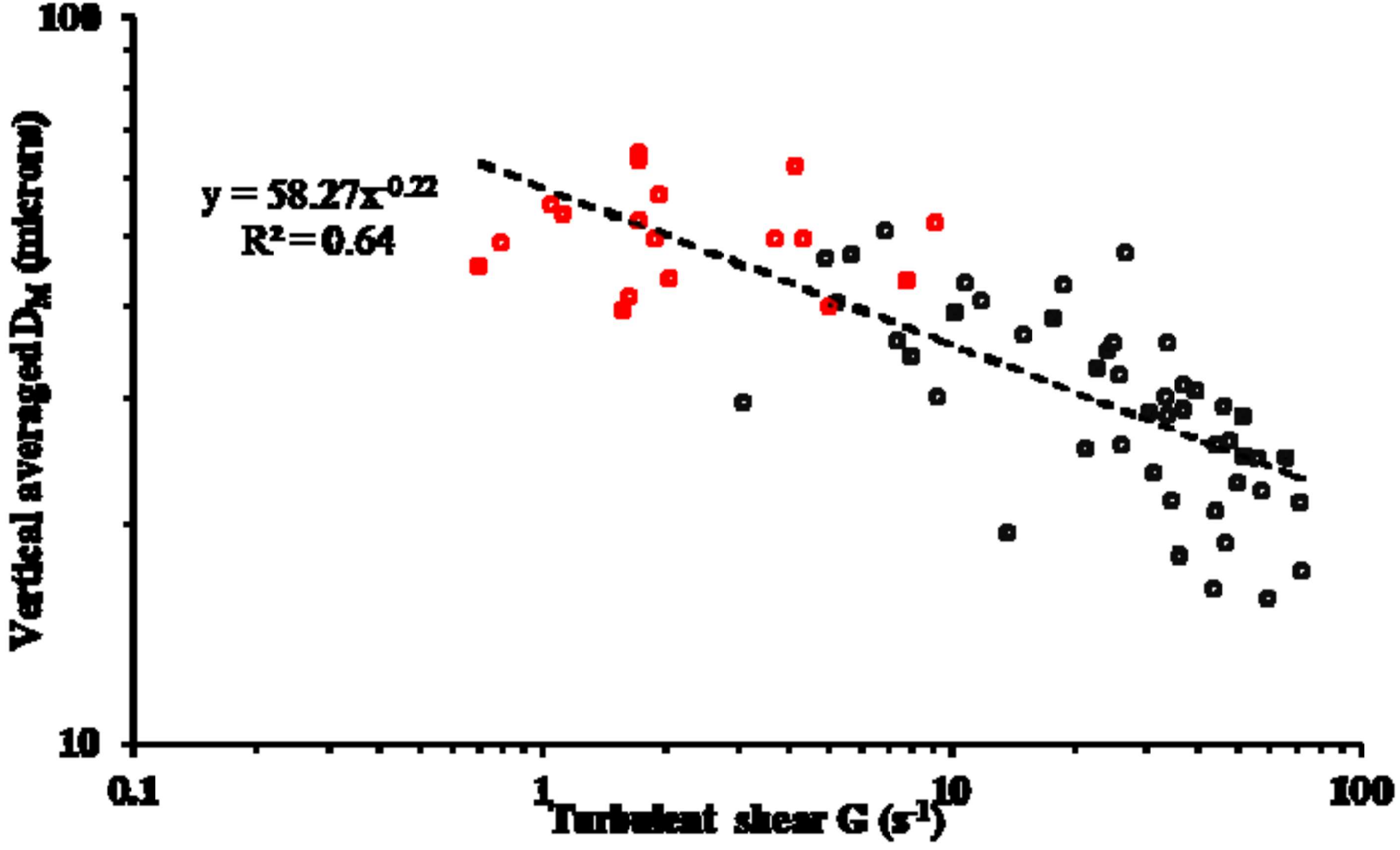
y = 58.27x^-0.22
R² = 0.64
100
10
0.1
1
10
100
Vertical averaged D_M (microns)
Turbulent shear G (s^-1)

Click here to download high resolution image

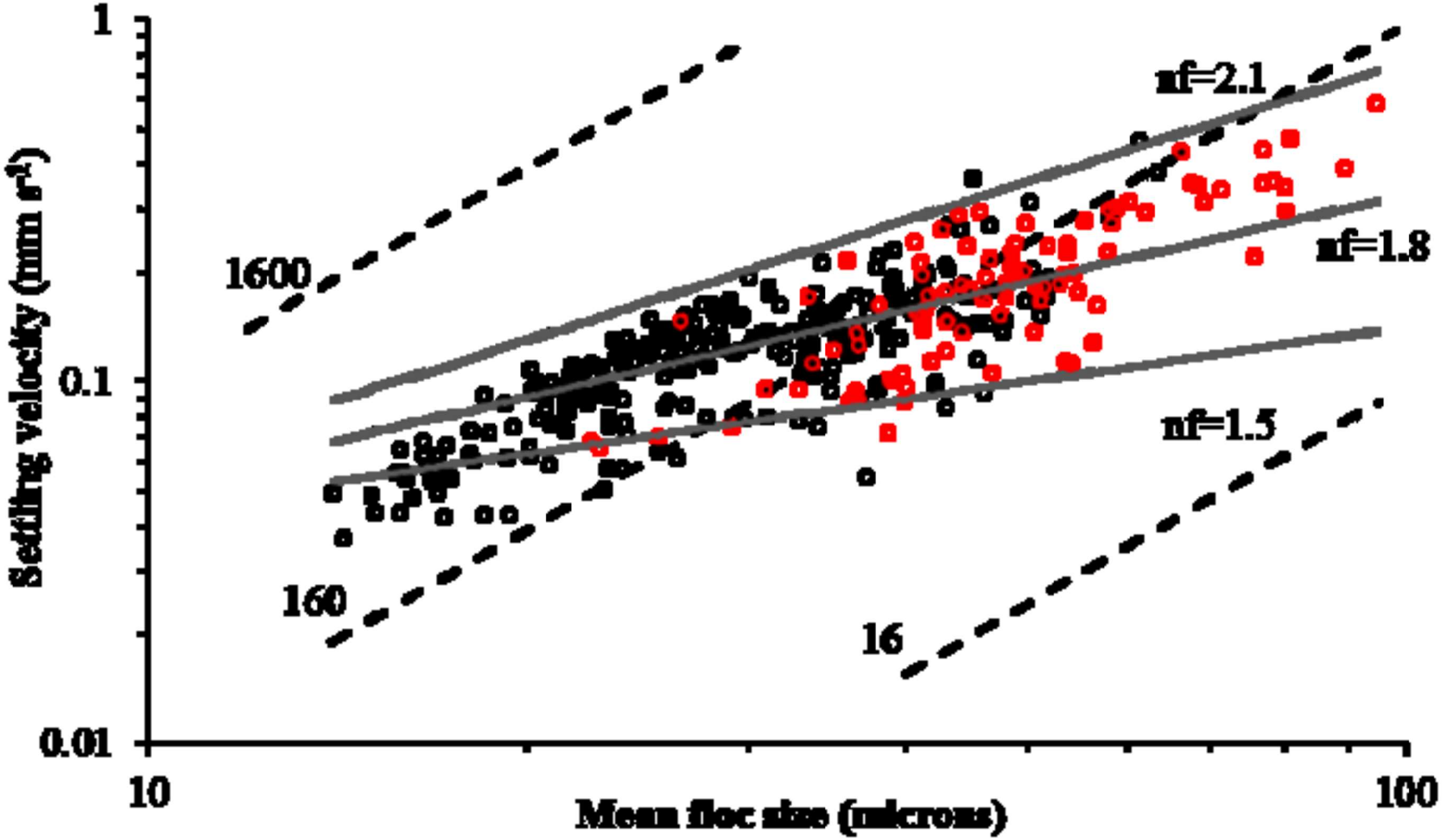

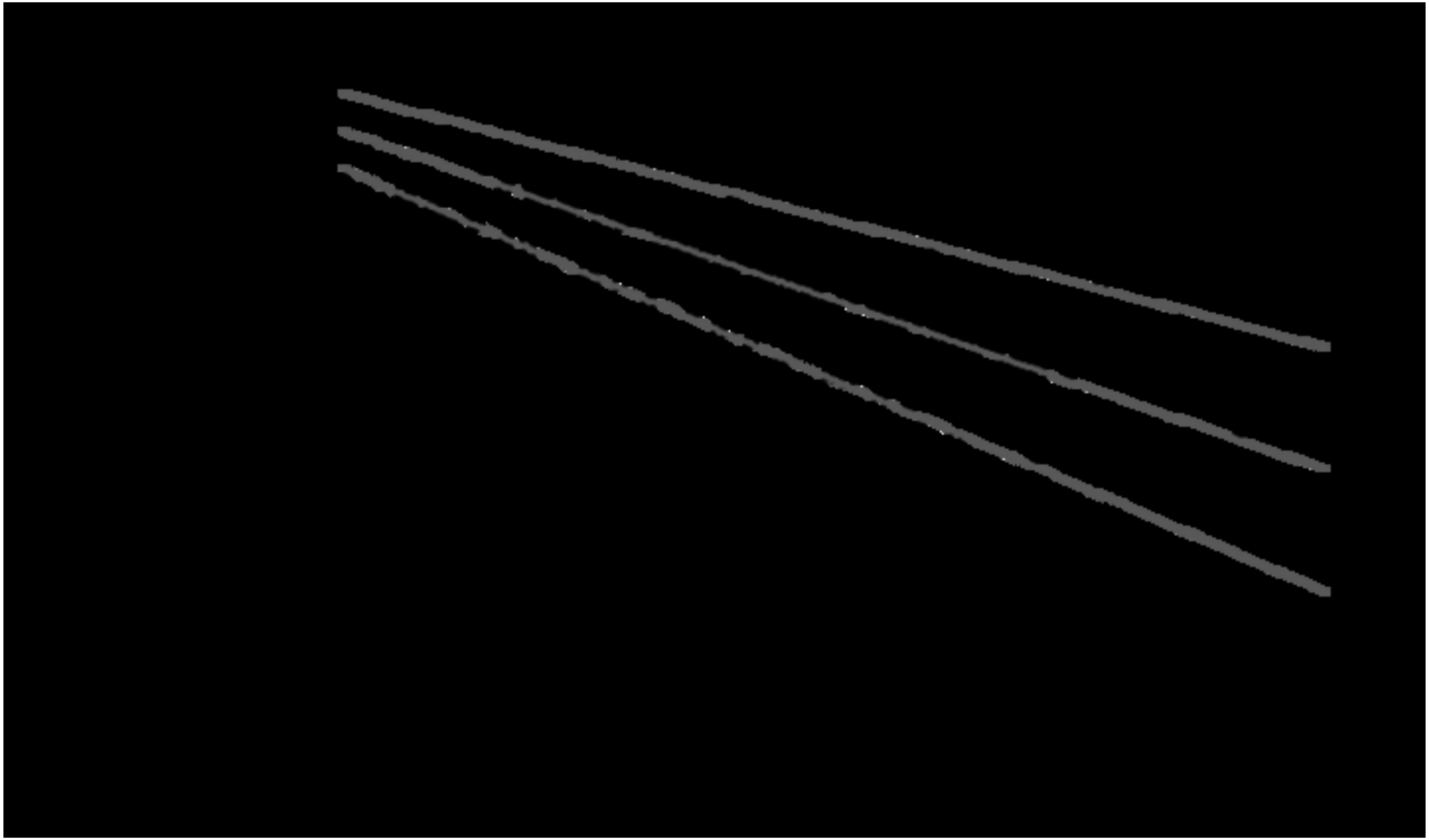

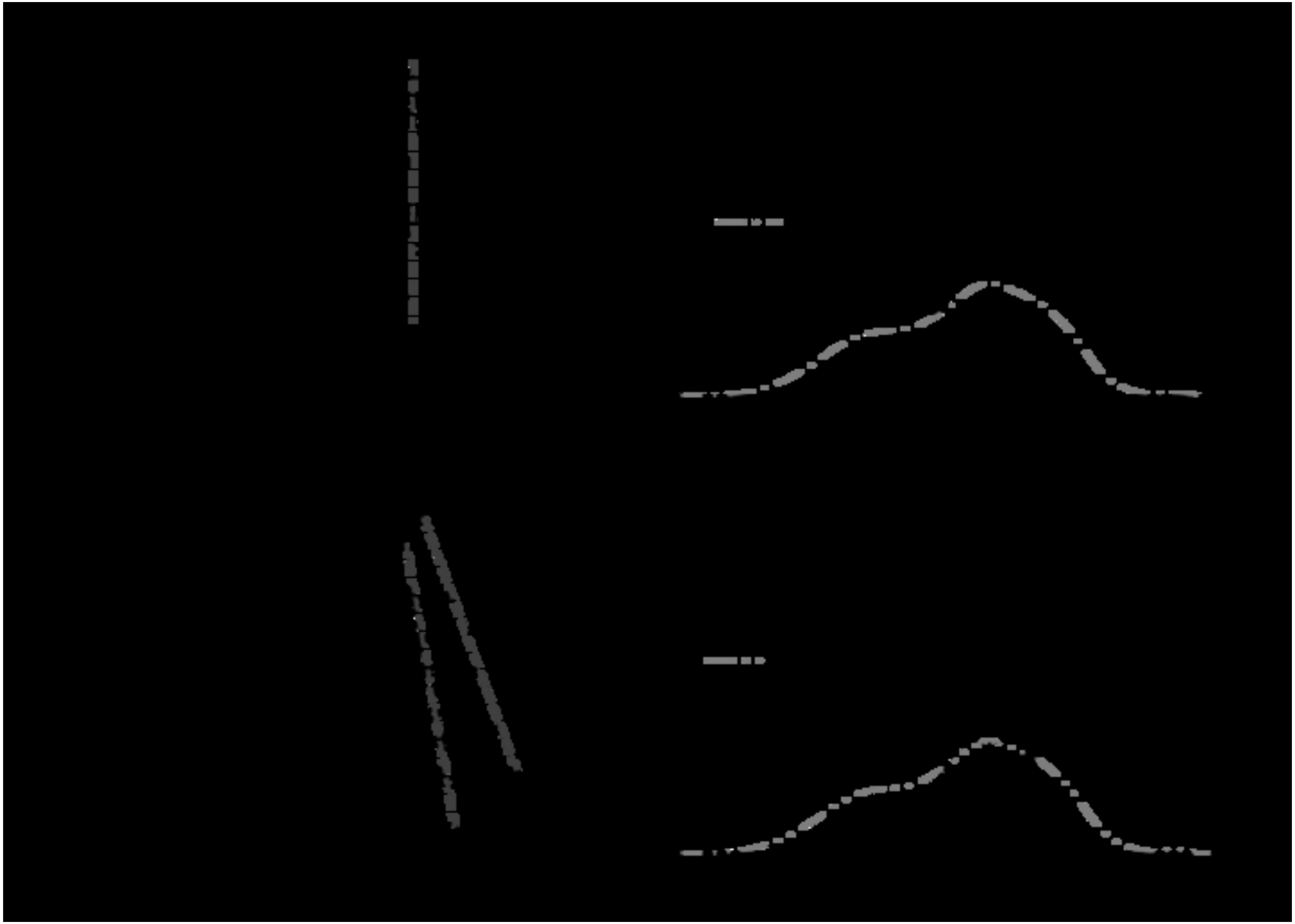

Click here to download high resolution image

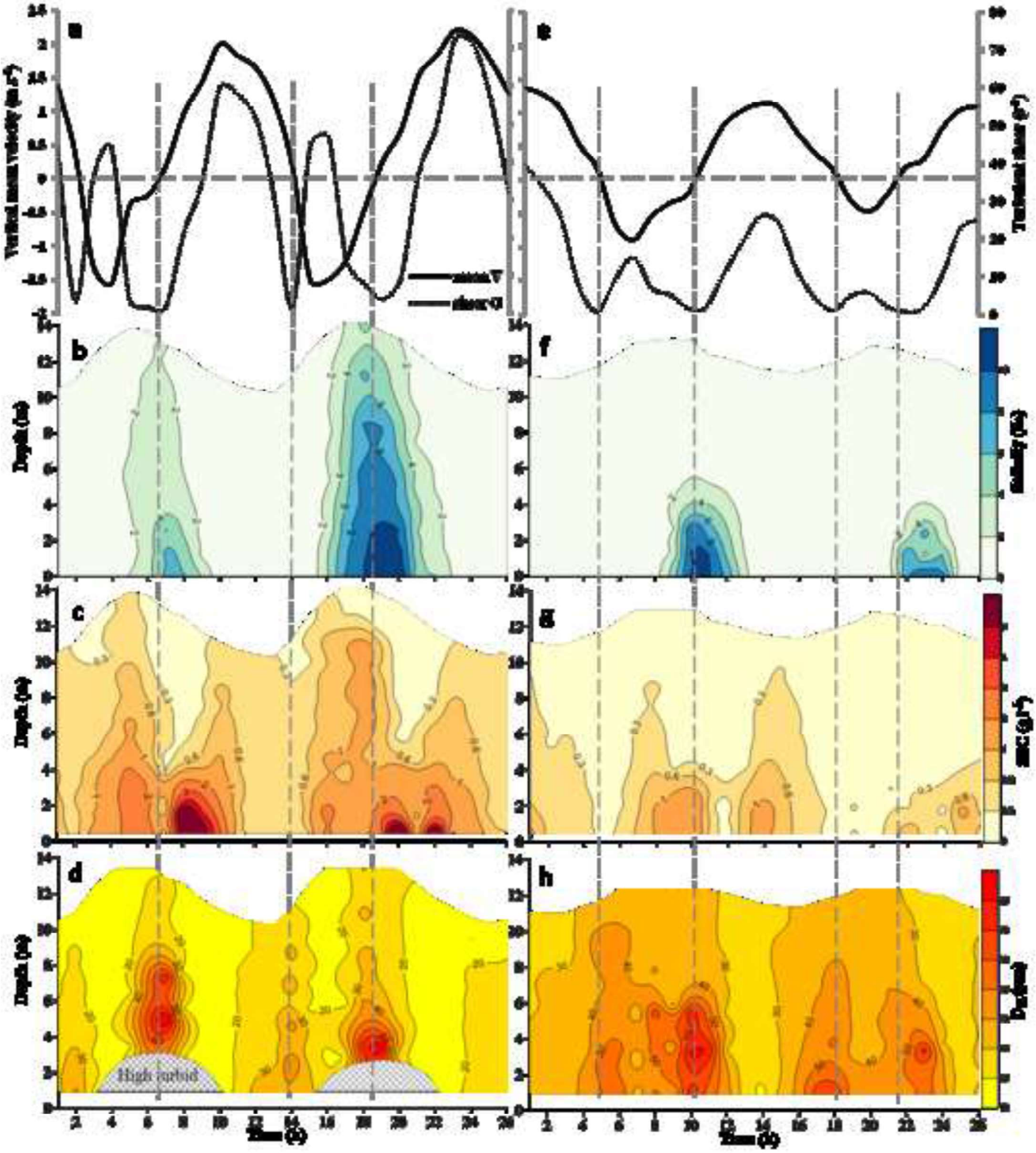

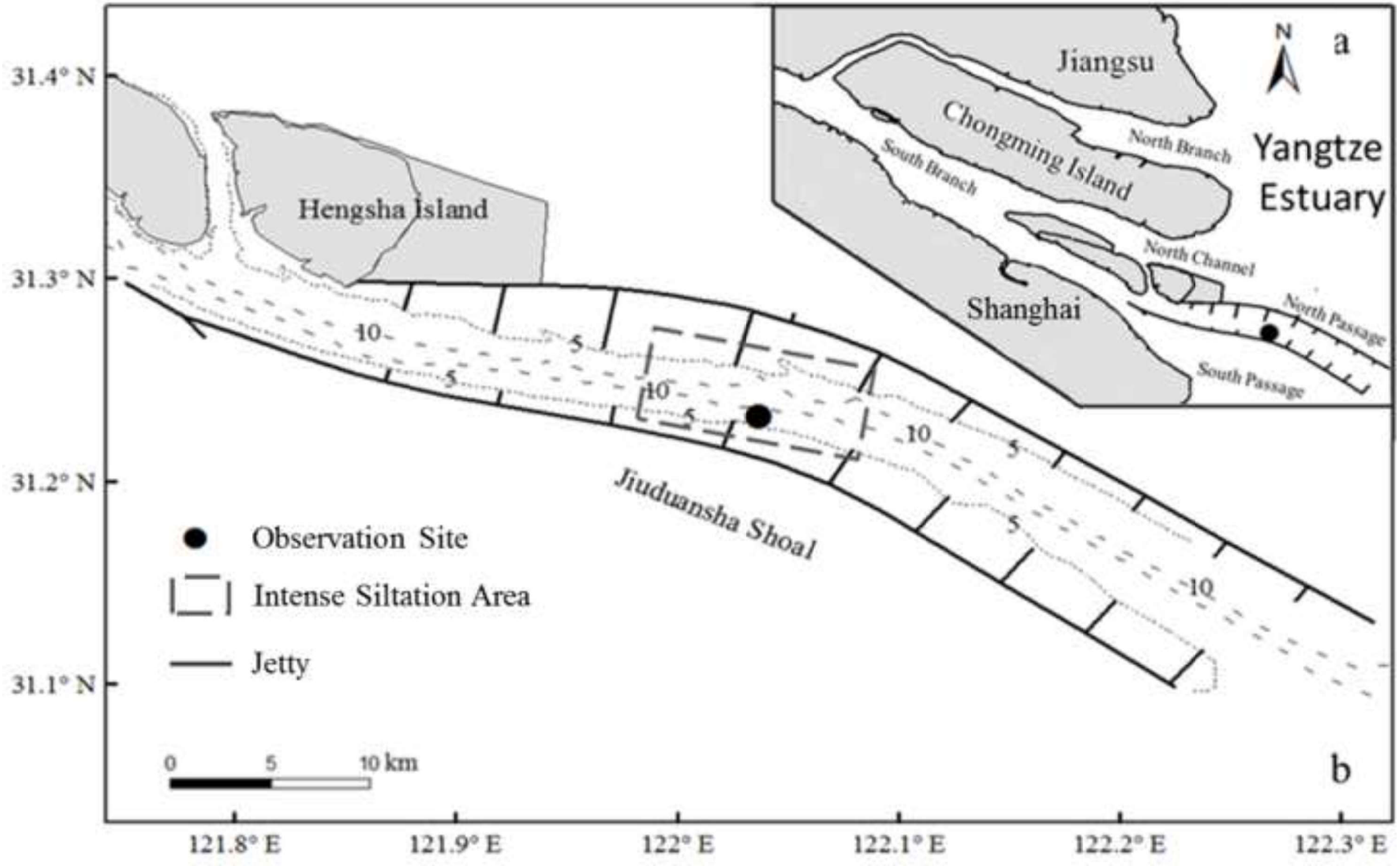
Jiangsu
Chongming Island
North Branch
South Branch
North Channel
Shanghai
North Passage
South Passage
N
a
Yangtze
Estuary
Hengsha Island
Jiuduansha Shoal
10
5
Observation Site
Intense Siltation Area
Jetty
0
5
10 km
b
31.4° N
31.3° N
31.2° N
31.1° N
121.8° E
121.9° E
122° E
122.1° E
122.2° E
122.3° E